K-Shell Photoelectric Cross Sections from 200 keV to 2 MeV†

R. H. Pratt*

Institute of Theoretical Physics, Department of Physics, Stanford University, Stanford, California

AND

Richard D. Levee,‡ Robert L. Pexton, and Walter Aron

Lawrence Radiation Laboratory, University of California, Livermore, California

(Received 13 September 1963)

A numerical program has been developed for the calculation of atomic photoelectric differential and total cross sections, including all polarization correlations. The program is designed to calculate relativistic Coulomb wave functions in a screened central potential; the outgoing continuum wave function is obtained in a partial-wave series. Results are presented here for K-shell differential and total cross sections in point Coulomb potentials (i.e., unscreened) ranging from charge $Z=13$ to $Z=92$, and covering the range of incident photon energies from 200 keV to 2 MeV. Enough data are presented to permit interpolation throughout these ranges. The total cross sections above 1 MeV are found to be significantly lower than previously accepted values. Further, the angular distributions from heavy elements deviate greatly from the commonly used Sauter distribution. These features are discussed and compared with existing experimental and theoretical work.

I. INTRODUCTION

ACCURATE predictions of the cross sections for the atomic photoelectric effect have in general been unavailable. Except for special limiting cases results must be obtained by numerical methods, even when the electron wave functions are assumed to be hydrogen-like and so available in analytic form. The complexity of these procedures has encouraged the use of extrapolation formulas based on various analytic approximations and indeed, at least for the total cross sections, moderate agreement with experiment has been obtained over a wide energy range.[1] The availability of accurate experimental total cross sections, the increasing need for accurate predictions of the differential cross sections, and the recent interest in the polarization properties of these reactions, have encouraged us to attempt their calculation by numerical means.[2]

We calculate in the central-field approximation, that is, we assume any atomic electron, whether bound or continuum, interacts only with a scalar spherically sym-

metric potential. Further, we neglect the effects of finite nuclear size, so that for sufficiently small distances this potential must simply reduce to the pure Coulomb Ze^2/r potential. For most applications these assumptions are appropriate.

Under these circumstances the theory of the atomic photoelectric effect is a simple application of first-order radiation theory. We require a fully relativistic treatment, since even at low energies, relativistic effects can be significant in a high-Z element. Then the differential cross section for the photoeffect is[1]

$$d\sigma/d\Omega = (2\pi)^{-2}p\epsilon|H|^2 \qquad (1.1)$$

subject to energy conservation, where

$$H = -e(2\pi/k)^{1/2}\int d^3r\psi_{\text{fin}}{}^*\boldsymbol{\alpha}\cdot\mathbf{e}e^{i\mathbf{k}\cdot\mathbf{r}}\psi_{\text{in}}. \qquad (1.2)$$

The absorbed radiation is described by its momentum $\mathbf{k}$ and polarization $\mathbf{e}$. ψ_{in} is a solution of the Dirac equation in a central potential corresponding to an initial bound state and ψ_{fin} is a solution corresponding to an outgoing electron of definite momentum $\mathbf{p}$ and energy ϵ ("plane wave" plus *ingoing* spherical waves).

Given the central potential, the entire problem is to solve the Dirac equation for the desired wave functions and then to integrate to obtain the matrix elements H. We have constructed a code for the IBM-7090 which does this.

In the present paper we present results for photoeffect from the K shell of an atom, obtained using wave functions in the pure point Coulomb field. The range of elements from aluminum ($Z=13$) to uranium ($Z=92$) was investigated for photon energies k from 200 keV to 2 MeV. Enough data were taken to permit interpolation throughout these ranges. For each choice of Z and k we obtained (1) the total cross section, (2) the differential cross section, and (3) all polarization correlations be-

[1] We will make some references to the previous work in this field in succeeding sections. The status of the subject up to 1954 is summarized for instance in W. Heitler, *Quantum Theory of Radiation* (Oxford University Press, New York, 1954), 3rd ed. We, in general, follow the notation of this book, but throughout we shall use the units $\hbar=c=m_e=1$. Thus, distances are measured in units of the electron compton wave length, etc. We will often use $a\equiv Ze^2$.

[2] While this work was in progress, an independent numerical calculation of K-shell photoelectric cross sections was reported by S. Hultberg, B. Nagel, and P. Olsson, Arkiv Fysik **20**, 555 (1961), hereafter referred to as HNO. This calculation, although using a method which cannot be applied to screened potentials and not obtaining results above 662 keV, is very valuable both for the information it provided on photoeffect at the lower energies and because it provides checking points for subsequent calculations, such as the present work.

tween incident photon and ejected electron. Results for differential and total cross sections are given here; the results obtained for the polarization correlations will be reported separately.[3] Most of the information is presented in tabular form. Modifications caused by screening,[4] extensions to lower and higher energies, and photoeffect from higher shells will be discussed in subsequent work.

The organization of the present paper is then as follows. In Sec. II we discuss the general properties of the photoeffect, as revealed by simple analytic approximations, and then develop the complete mathematical formalism for the process. Section III is devoted to a short discussion of the numerical methods for calculating wave functions, some features of which have not previously been published. The accuracy of the numerical calculations is discussed in Sec. IV. The remainder of the paper presents our results and compares them with experiment and previous theory. This is done for the total cross section in Sec. V and for the differential cross sections in Sec. VI.

II. GENERAL PROPERTIES AND FORMALISM

The main purpose of this section is to develop the formalism, based on Eqs. (1.1) and (1.2), needed for the calculation of the photoeffect. The wave function ψ_{fin} for the outgoing electron must be written as a sum over partial waves with appropriate asymptotic properties. Then for each partial wave the integrations over angles of Eq. (1.2) may be performed analytically, leaving a small number of radial integrals to be done numerically. The cross sections and the polarization correlations will be completely specified by these quantities.

It is useful, however, to first have a qualitative understanding of the general features of the process. For this purpose we replace Eq. (1.2) with the corresponding nonrelativistic expression

$$H = -e(2\pi/k)^{1/2} \int d^3r \, \psi_{\text{fin}}^* \mathbf{p} \cdot \mathbf{e} e^{i\mathbf{k}\cdot\mathbf{r}} \psi_{\text{in}}. \quad (2.1)$$

We assume a pure Coulomb potential, so that for photoeffect from the K shell $\psi_{\text{in}} = (a^3/\pi)^{1/2} e^{-ar}$, where $a \equiv Ze^2$. We also make the Born approximation and replace ψ_{fin} with the plane wave $e^{i\mathbf{p}\cdot\mathbf{r}}$. Then the integral (2.1) is easily done, and the differential cross section for photo effect from *both* K-shell electrons is given as

$$\frac{d\sigma}{d\Omega} = 4e^2 a^5 (e_1 e_1^*) \frac{p^3}{k^5 \epsilon^3} \frac{\sin^2\theta}{(1 - \beta \cos\theta)^4}, \quad (2.2)$$

where θ is the angle between $\mathbf{k}$ and $\mathbf{p}$, and e_1 is the component of the photon polarization vector in the scattering plane which $\mathbf{k}$ and $\mathbf{p}$ define.

This cross section vanishes both in the forward and backward directions. For low energies ($\beta \ll 1$) it has a broad maximum centered at $\theta = 90°$; as the energy increases the maximum shifts toward smaller angles and its width decreases. Equation (2.2) is independent of any circular polarization of the incident photons, but it is sensitive to linear polarization: If the beam is linearly polarized in the direction $\mathbf{e}$, $e_1 = \cos\varphi$, where φ is the angle between the plane of $\mathbf{k}$ and $\mathbf{p}$ and the plane of $\mathbf{k}$ and $\mathbf{e}$; there is no emission perpendicular to the direction of polarization. Integrating over angles, the total cross section for unpolarized photons of low energy (but far above threshold) reduces to

$$\sigma = 32\sqrt{2}\pi e^2 a^5 / 3k^{7/2}. \quad (2.3)$$

We note that this (1) varies as the *fifth* power of Z and (2) decreases rapidly with increasing energy.

These results must be modified both for low and for high energies. Near threshold the Born approximation expansion in a/β is invalid; when the exact nonrelativistic Coulomb wave functions are used it is found[1] that the total cross section (2.3) must be multiplied by

$$f = 2\pi \left(\frac{I}{k}\right)^{1/2} \frac{e^{-4\eta \cot^{-1}\eta}}{1 - e^{-2\pi\eta}}, \quad \eta = [I/(k-I)]^{1/2}, \quad (2.4)$$

where I is the ionization energy. This causes an appreciable reduction from the Born approximation prediction, which is reached only slowly as the energy increases, in the entire low-energy region; at the K-shell threshold $f = 0.12$.[5]

For higher energies a relativistic treatment based on Eq. (1.2) is necessary. Sauter found that, to lowest order in Z, the differential cross section from linearly polarized photons is given by[6]

$$\frac{d\sigma}{d\Omega} = 4e^2 a^5 \frac{p^3}{k^5 \epsilon^4} \left[\frac{\sin^2\theta \cos^2\varphi}{(1 - \beta \cos\theta)^4} - \frac{1 - (1-\beta^2)^{1/2}}{2(1-\beta^2)} \frac{\sin^2\theta \cos^2\varphi}{(1 - \beta \cos\theta)^3} \right.$$
$$\left. + \frac{[1 - (1-\beta^2)^{1/2}]^2}{4(1-\beta^2)^{3/2}} \frac{\sin^2\theta}{(1 - \beta \cos\theta)^3} \right]. \quad (2.5)$$

This again vanishes in the forward and backward directions; the maximum narrows and moves toward the forward direction as the energy increases. There is now some emission perpendicular to the direction of polariza-

[3] R. H. Pratt, R. D. Levee, R. L. Pexton, and W. Aron, Phys. Rev. **134**, A916 (1964) (following paper).

[4] For K-shell photoeffect, it is believed that screening effects are quite small, typically (in heavy elements) of the order of 1–2%. For all other shells, screening effects are large and the use of hydrogen-like wave functions in a numerical calculation is not justified.

[5] However, in heavy elements relativistic effects are important at threshold. Part of this is simply due to the relativistic shift of the threshold energy. The relativistic K-shell photoeffect at threshold has been discussed by B. Nagel and P. Olsson, Arkiv Fysik **18**, 29 (1960), in the approximation of an unscreened point Coulomb potential. However, as the authors note, screening effects are expected to be significant in the threshold region even for K-shell photoeffect.

[6] F. Sauter, Ann. Physik **11**, 454 (1931).

tion. For very high energies the total cross section from unpolarized photons becomes

$$\sigma = 4\pi e^2 a^5/k, \tag{2.6}$$

and so still varies with the fifth power of Z but decreases less rapidly with increasing energy.

For high-Z elements the corrections to this lowest order theory can be very large. The high-energy behavior of the total cross section has been obtained exactly,[7] with numerical methods, and for $Z=82$ (lead) the prediction of Eq. (2.6) is too large by a factor of five. The expression

$$\sigma = [4\pi e^2 a^5/k] e^{-\pi a} (1 - 4\pi a/15), \tag{2.7}$$

derived analytically, is in fair agreement with these results, and shows the nature of the suppression of the Z^5 dependence. It has also been shown that the cross section does not vanish in the forward direction when terms of relative order a^2 are considered, and such effects have been observed experimentally.[1]

In relativistic photoeffect there will also be interactions with the electron spin, and hence many more types of polarization correlations are possible. To describe these it is convenient to introduce the usual polarization parameters. We describe photon polarization with the quantities

$$\xi_1 = e_1^* e_1 - e_2^* e_2, \quad \xi_2 = e_1 e_2^* + e_2 e_1^*, \\ \xi_3 = i(e_1 e_2^* - e_2 e_1^*), \tag{2.8}$$

and we describe the polarization of the ejected electron by the direction ζ of its spin in its rest system. ζ_3 is taken along $\mathbf{p}$, ζ_1 in the scattering plane. Then if we sum or average over the initial polarization states of the bound electron, the differential cross section for photoeffect must be of the form

$$\frac{d\sigma}{d\Omega} = \left(\frac{d\sigma}{d\Omega}\right)_{\text{unpol}} \left[\frac{1}{2} \sum_{i,j=0}^{3} \xi_i \zeta_j C_{ij}\right], \tag{2.9}$$

where $\xi_0 = \zeta_0 = C_{00} = 1$, and $(d\sigma/d\Omega)_{\text{unpol}}$ is the differential cross section from unpolarized photons, summed over final electron spins. The correlation C_{10} connects linearly polarized photons and unpolarized electrons, and as already noted, occurs in the lowest order cross section. Also occurring in lowest order are C_{33}, connecting longitudinally polarized electrons and transversely polarized photons, and C_{31}. The correlations C_{02}, C_{12}, C_{21}, and C_{23} appear in relative order a. The remaining correlations are forbidden by invariance considerations.

We can now develop the formalism needed for a numerical calculation of these photoeffect cross sections. To begin with, we need wave functions for the electrons. A bound state will be specified by *capital* letters: total angular momentum J, orbital angular momentum L, $(J=L\pm\frac{1}{2})$, the azimuthal quantum number M, and

[7] R. H. Pratt, Phys. Rev. **117**, 1017 (1960).

total energy (including rest mass energy) E. Thus, for ψ_{in} in Eq. (1.2) we write

$$\psi_{\text{in}} = \begin{pmatrix} G_\kappa(r) & \Omega_{JLM}(\hat{r}) \\ iF_\kappa(r) & \Omega_{JL'M}(\hat{r}) \end{pmatrix}, \tag{2.10}$$

where L' and κ are defined by

$$L + L' = 2J,$$
$$\kappa = \mp(J+\tfrac{1}{2}) \text{ as } J = L\pm\tfrac{1}{2}, \quad (\text{or } J = L'\mp\tfrac{1}{2}), \tag{2.11}$$

and the spherical spinors Ω_{JLM} are defined in terms of spherical harmonics[8] by

$$\Omega_{JLM} = \begin{pmatrix} C_{JLM}^+ & Y_{L,M-\frac{1}{2}} \\ C_{JLM}^- & Y_{L,M+\frac{1}{2}} \end{pmatrix}, \tag{2.12}$$

where

$$J = L + \tfrac{1}{2} \qquad J = L - \tfrac{1}{2}$$

$$C^+ = \left[\frac{J+M}{2L+1}\right]^{1/2} \quad \left[\frac{J-M+1}{2L+1}\right]^{1/2};$$
$$\tag{2.13}$$
$$C^- = \left[\frac{J-M}{2L+1}\right]^{1/2} \quad \left[\frac{J+M+1}{2L+1}\right]^{1/2}.$$

The radial functions G_κ and F_κ are to be obtained as solutions of the coupled equations

$$[E+1+\varphi]F_\kappa - [dG_\kappa/dr + (1+\kappa)(G_\kappa/r)] = 0,$$
$$[E-1+\varphi]G_\kappa + [dF_\kappa/dr + (1-\kappa)(F_\kappa/r)] = 0. \tag{2.14}$$

The potential φ must be specified (for the pure Coulomb potential $\varphi = a/r$) and the energy E is then determined from the eigenvalue problem. The wave function will be normalized by requiring

$$\int r^2 dr [(F)^2 + (G)^2] = 1. \tag{2.15}$$

The wave function ψ_{fin} of the outgoing continuum electron is written as a sum over partial-wave solutions with appropriate asymptotic properties:

$$\psi_{\text{fin}} = \sum_{jlm} 4\pi (\Omega_{jlm}^+(\hat{p}) U_A) i^l e^{-i\delta_\kappa} \begin{pmatrix} g_\kappa \Omega_{jlm}(\hat{r}) \\ if_\kappa \Omega_{jl'm}(\hat{r}) \end{pmatrix}. \tag{2.16}$$

Equations (2.10)–(2.14) are understood to remain valid with the substitution of the *small* letters j, l, l', m, κ, ϵ, etc., and of course $p^2 + 1 = \epsilon^2$, where $\mathbf{p}$ is the momentum of the outgoing particle. The two-spinor U_A specifies the polarization properties of the electron in its rest frame. Equation (2.15), however, is not appropriate for continuum functions, and is replaced by the requirement that the functions are normalized such that at large

[8] We use the phase conventions of A. R. Edmonds, *Angular Momentum in Quantum Mechanics* (Princeton University Press, Princeton, New Jersey, 1957).

distances

$$g_\kappa \xrightarrow[r\to\infty]{} \left(\frac{\epsilon+1}{2\epsilon}\right)^{1/2}\frac{1}{pr}\sin(pr-\tfrac{1}{2}l\pi+\delta_\kappa),$$

$$f_\kappa \xrightarrow[r\to\infty]{} \left(\frac{\epsilon-1}{2\epsilon}\right)^{1/2}\frac{1}{pr}\cos(pr-\tfrac{1}{2}l\pi+\delta_\kappa).$$

(2.17)

Equation (2.17) also defines the phase shifts δ_κ. [For the pure Coulomb potentials δ_κ in Eq. (2.17) but *not* Eq. (2.16) should be replaced by $\delta_\kappa+(a\epsilon/p)\ln 2pr$—this feature arises from the long-range character of the potential.] Note that the sum over j and l subject to $j=l\pm\frac{1}{2}$ in Eq. (2.16) is equivalent to a single sum over κ, where κ ranges over all positive and negative integers.

Substituting the wave functions (2.10) and (2.16) back into Eq. (1.2), H can be written as a summation of terms, each corresponding to a given κ and m in the series for the continuum wave function. It is convenient to remove some constants and write this in the form

$$H=-e(2\pi/k)^{1/2}\sum_\kappa \mathfrak{IC}_\kappa,$$

(2.18)

where each $\mathfrak{IC}_\kappa$ represents a sum over all m values consistent with that κ.

Now we choose a z axis along the photon direction $\mathbf{k}$ and start performing the angular integrations. In the φ integration nonvanishing contributions come only for $m=M\pm1$, and thus the summation over m implied in $\mathfrak{IC}_\kappa$ reduces to two terms. This is most conveniently written in terms of the circular polarization coefficients $e_\pm\equiv e_x\pm ie_y$, for then

$$\mathfrak{IC}_\kappa=4\pi e^{i\delta_\kappa}[(U_A{}^*\Omega_{jlM+1}(\hat{p}))e_-R_\kappa{}^+(M)$$
$$+(U_A{}^*\Omega_{jlM-1}(\hat{p}))e_+R_\kappa{}^-(M)], \quad (2.19)$$

where the R's, a set of numbers resulting from θ and r integrations contain all the remaining information of the problem. (R's of $\pm M$ are easily related.) To proceed further for an arbitrary bound state one expands the plane wave $e^{i\mathbf{k}\cdot\mathbf{r}}$ of Eq. (1.2) in spherical harmonics and then integrates over products of three spherical harmonics.

For the purpose of this paper we restrict our attention to bound S states ($J=\frac{1}{2}$, $L=0$) and the results are quite simple. All the information of the problem is contained in two sets of numbers, $R_\kappa{}^\pm$, defined by

$$R_\kappa{}^+=\int r^2 dr\, g_\kappa F_\kappa C_{jl+\frac{3}{2}}{}^+\left[\frac{l(l+1)}{2l+1}\right]^{1/2}$$
$$\times[j_{l-1}(kr)+j_{l+1}(kr)],$$

$$R_\kappa{}^-=\int r^2 dr\Bigg\{g_\kappa F_\kappa C_{jl-\frac{1}{2}}{}^-$$

(2.20)

$$\times\left[-j_{l-1}(kr)\left(\frac{l^2}{(2l+1)}\right)^{1/2}+j_{l+1}(kr)\left(\frac{(l+1)^2}{2l+1}\right)^{1/2}\right]$$
$$+\eta_\kappa f_\kappa G_\kappa C_{jl'-\frac{1}{2}}{}^-(2l'+1)^{1/2}j_{l'}(kr)\Bigg\},$$

where $\eta_\kappa=\pm1$ according as $j=l\mp\frac{1}{2}$. [These R's correspond to $R^\pm(M=+\frac{1}{2})$ of Eq. (2.19).] Then for $M=+\frac{1}{2}$

$$\mathfrak{IC}_\kappa=4\pi e^{i\delta_\kappa}[(U_A{}^*\Omega_{jl+\frac{1}{2}}(\hat{p}))e_-R_\kappa{}^+$$
$$+(U_A{}^*\Omega_{jl-\frac{1}{2}}(\hat{p}))e_+R_\kappa{}^-], \quad (2.21)$$

and for $M=-\frac{1}{2}$

$$\mathfrak{IC}_\kappa=-4\pi\eta_\kappa e^{i\delta_\kappa}[(U_A{}^*\Omega_{jl-\frac{1}{2}}(\mathbf{p}))e_+R_\kappa{}^+$$
$$+(U_A{}^*\Omega_{jl+\frac{1}{2}}(\hat{p}))e_-R_\kappa{}^-]. \quad (2.22)$$

We shall *sum* over the two electrons of a bound S state. Then the differential cross section for a photon with polarization parameter ξ_i [as in Eq. (2.8)] to eject an electron with spin direction ζ (in its rest system, with ζ_3 chosen along the electron, and ζ_1 in the scattering plane) into the solid angle $d\Omega$ may be written

$$\frac{d\sigma}{d\Omega}=\tfrac{1}{2}A\sum_{i,j=0}^{3}\xi_i\zeta_j B_{ij},$$

(2.23)

where

$$\xi_0=\zeta_0=1, \quad A=16\pi e^2 p\epsilon/k.$$

(2.24)

The only nonvanishing B's are

$$B_{00}=[|J_-|^2+|K_-|^2+|J_+|^2+|K_+|^2],$$
$$B_{02}=2\operatorname{Im}[J_-{}^*K_-+J_+{}^*K_+],$$
$$B_{10}=2\operatorname{Re}[J_-{}^*J_++K_-{}^*K_+],$$
$$B_{12}=2\operatorname{Im}[J_-{}^*K_++J_+{}^*K_-],$$
$$B_{21}=-2\cos\theta\operatorname{Im}[J_-{}^*K_++K_-{}^*J_+]$$
$$+2\sin\theta\operatorname{Im}[J_-{}^*J_++K_+{}^*K_-], \quad (2.25)$$
$$B_{23}=-2\cos\theta\operatorname{Im}[J_-{}^*J_++K_+{}^*K_-]$$
$$-2\sin\theta\operatorname{Im}[J_-{}^*K_++K_-{}^*J_+],$$
$$B_{31}=2\cos\theta\operatorname{Re}[J_-{}^*K_--J_+{}^*K_+]$$
$$-\sin\theta[|J_-|^2-|K_-|^2+|K_+|^2-|J_+|^2],$$
$$B_{33}=\cos\theta[|J_-|^2-|K_-|^2+|K_+|^2-|J_+|^2]$$
$$+2\sin\theta\operatorname{Re}[J_-{}^*K_--J_+{}^*K_+],$$

where

$$J_-=-(4\pi)^{-1/2}\sum_\kappa \eta_\kappa e^{i\delta_\kappa}\left[\frac{|\kappa-1|}{|\kappa||\kappa+1|}\right]^{1/2}R_\kappa{}^+P_l{}^1(\cos\theta),$$

$$K_-=(4\pi)^{-1/2}\sum_\kappa e^{i\delta_\kappa}[|\kappa||\kappa^2-1|]^{-1/2}R_\kappa{}^+P_l{}^2(\cos\theta),$$

(2.26)

$$J_+=(4\pi)^{-1/2}\sum_\kappa \eta_\kappa e^{i\delta_\kappa}[|\kappa|]^{-1/2}R_\kappa{}^-P_l{}^1(\cos\theta),$$

$$K_+=(4\pi)^{-1/2}\sum_\kappa e^{i\delta_\kappa}[|\kappa|]^{1/2}R_\kappa{}^-P_l{}^0(\cos\theta).$$

In the sums of Eq. (2.26) terms for which the P_l's do not exist are to be omitted; θ is the angle between photon direction $\mathbf{k}$ and electron direction $\mathbf{p}$. [The last four B's of Eq. (2.25) take their form when a rotation is made so that ζ_3 refers to a spin along the *electron* direction.] To put our result in the form of Eq. (2.9) we finally define the polarization correlations by

$$C_{ij}\equiv B_{ij}/B_{00}.$$

(2.27)

The differential cross section from unpolarized photons, summed over electron spins is then

$$\left(\frac{d\sigma}{d\Omega}\right)_{\text{unpol}} = AB_{00} \qquad (2.28)$$

and the total cross section

$$\sigma = 2\pi A \int_0^\pi B_{00} \sin\theta d\theta = A \sum_\kappa \left[(R_\kappa^+)^2 + (R_\kappa^-)^2\right]. \qquad (2.29)$$

Thus, when the quantities $R_\kappa^\pm$ (and the phase shifts δ_κ) have been calculated, all properties of the process may be predicted. And the main work in calculating these quantities lies in the prior calculation of the electron wave functions.

III. METHOD OF SOLUTION OF THE WAVE EQUATIONS

A. The Bound-State Wave Equations

The bound-state wave equations

$$\begin{aligned}
(E+1+\varphi)F_\kappa - [dG_\kappa/dr + (1+\kappa)(G_\kappa/r)] &= 0, \\
(E-1+\varphi)G_\kappa + [dF_\kappa/dr + (1-\kappa)(F_\kappa/r)] &= 0,
\end{aligned} \qquad (3.1)$$

constitute an eigenvalue problem for the energy eigenvalue E and the bound-state wave functions F_κ, G_κ. Since F_κ and G_κ behave like $r^{\gamma-1}$ near $r=0$ for the Coulomb potential[9] and are therefore singular for $\gamma<1$, it is convenient to make the substitution

$$G_\kappa = \bar{G}_\kappa r^{\gamma-1}, \quad F_\kappa = \bar{F}_\kappa r^{\gamma-1}.$$

Equations (3.1) then become

$$\begin{aligned}
(E+1+\varphi)\bar{F}_\kappa - \left[\frac{d\bar{G}_\kappa}{dr} + \frac{(\gamma+\kappa)}{r}\bar{G}_\kappa\right] &= 0, \\
(E-1+\varphi)\bar{G}_\kappa + \left[\frac{d\bar{F}_\kappa}{dr} + \frac{(\gamma-\kappa)}{r}\bar{F}_\kappa\right] &= 0,
\end{aligned} \qquad (3.2)$$

where $\bar{F}_\kappa$ and $\bar{G}_\kappa$ are finite at $r=0$.

Although the following analysis for the solution of Eqs. (3.2) applies to a potential φ of any form, we shall in the present paper specify the Coulomb potential $\varphi = a/r$.

The boundary conditions associated with (3.2) with $\varphi = a/r$ are determined at the origin by multiplying through by r and letting $r=0$. We have then

$$\begin{aligned}
a\bar{F}_\kappa(0) - (\gamma+\kappa)\bar{G}_\kappa(0) &= 0, \\
a\bar{G}_\kappa(0) + (\gamma-\kappa)\bar{F}_\kappa(0) &= 0.
\end{aligned} \qquad (3.3)$$

Since the equations are linear and homogeneous, we may choose $\bar{G}_\kappa(0)$ arbitrarily equal to one. $\bar{F}_\kappa(0)$ is then

[9] L. I. Schiff, *Quantum Mechanics* (McGraw-Hill Book Company, Inc., New York, 1955), 2nd ed., Sec. 44, p. 336.

determined by either of the Eqs. (3.3), and γ is determined by the requirement that

$$\begin{vmatrix} a & -(\gamma+\kappa) \\ \gamma-\kappa & a \end{vmatrix} = 0$$

or

$$\gamma = (\kappa^2 - a^2)^{1/2}, \qquad (3.4)$$

where the positive sign is taken to obtain a physically acceptable wave function.

In order to determine E we need to satisfy the boundary condition at $r \to \infty$; that is we must approach the asymptotic solution of (3.2). This solution is determined by letting $r \to \infty$ in (3.2), leading to

$$\begin{aligned}
(E+1)\bar{F}_\kappa - \bar{G}'_\kappa &= 0, \\
(E-1)\bar{G}_\kappa + \bar{F}'_\kappa &= 0,
\end{aligned}$$

which have the solution

$$\begin{aligned}
\bar{G}_\kappa &= C_1 e^{-\lambda r}, \\
\bar{F}_\kappa &= C_2 e^{-\lambda r},
\end{aligned} \qquad (3.5)$$

where $\lambda = (1-E^2)^{1/2}$ with $E<1$. Increasing solutions are ruled out since the wave function must be bounded as $r \to \infty$. [In the point Coulomb potential, these forms must be multiplied by $r^{n-|\kappa|}$, where n is the principal quantum number; this has no effect for the K shell.]

In order to numerically integrate (3.2), we must replace them by suitable difference equations. In the difference equations we have chosen, we evaluate the wave functions $\bar{F}$ and $\bar{G}$ (for simplification we have dropped the subscript κ) at the discrete points labeled by integral values of j running from zero at $r=0$ to J at a point r_J. The coordinate r_J is that point where the asymptotic boundary conditions (3.5) are satisfied in appropriate difference form to within some tolerance T_1. The conditions (3.2) are applied at $j+\frac{1}{2}$ and the derivatives are therefore evaluated as the slope of the chords joining values at j and $j+1$. Quantities needed at $j+\frac{1}{2}$ are evaluated by averaging. The resulting finite difference equations are

$$(E+1+\varphi_{j+\frac{1}{2}})\frac{(\bar{F}_{j+1}+\bar{F}_j)}{2}$$

$$-\left[\frac{\bar{G}_{j+1}-\bar{G}_j}{r_{j+1}-r_j} + \frac{(\gamma+\kappa)}{2r_{j+\frac{1}{2}}}(\bar{G}_{j+1}+\bar{G}_j)\right] = 0,$$

$$(E-1+\varphi_{j+\frac{1}{2}})\frac{(\bar{G}_{j+1}+\bar{G}_j)}{2} \qquad (3.6)$$

$$+\left[\frac{\bar{F}_{j+1}-\bar{F}_j}{r_{j+1}-r_j} + \frac{(\gamma-\kappa)}{2r_{j+\frac{1}{2}}}(\bar{F}_{j+1}+\bar{F}_j)\right] = 0,$$

with $0 \le j \le J-1$.

The basis of the method is the simultaneous solution

of the complete set of difference equations and boundary conditions. This method has been described for a two-point boundary value problem by Henyey et al.[10] The suggestion that the method could also be used for eigenvalue problems was made to one of us by Henyey[11] many years ago and has in fact been used by Levee to solve many problems.

The Eqs. (3.6), although linear in the functions $\bar{F}$ and $\bar{G}$, are nonlinear in the unknowns because of the appearance of the eigenvalue E. They must therefore be solved by an iterative technique such as the Newton-Raphson method described in Henyey et al.[10]

Formally we may write (3.6) as

$$Q_{j+\frac{1}{2}}{}^1(\bar{F}_{j+1},\bar{F}_j,\bar{G}_{j+1},\bar{G}_j,E)=0,$$
$$Q_{j+\frac{1}{2}}{}^2(\bar{F}_{j+1},\bar{F}_j,\bar{G}_{j+1},\bar{G}_j,E)=0, \qquad (3.7)$$
$$0\le j\le J-1.$$

The Newton-Raphson method when applied to a system

$$f_k(x_1,x_2,\cdots,x_K)=0, \quad k=1, 2, \cdots, K \qquad (3.8)$$

corrects an approximate set of values $x_1{}^p, x_2{}^p, \cdots, x_K{}^p$ by variations $\delta x_1{}^p, \delta x_2{}^p, \cdots, \delta x_K{}^p$ to give improved values $x_1{}^{p+1}, x_2{}^{p+1}, \cdots, x_K{}^{p+1}$ where p is the iteration number. The variations are determined from the equations

$$f_k+\sum_{l=1}^{K}\frac{\partial f_k}{\partial x_l}\delta x_l=0, \quad k=1, 2, \cdots, K \qquad (3.9)$$

and the iteration is continued until the Eqs. (3.8) are satisfied to within some desired tolerance.

If we define the following two vectors

$$Q_{j+\frac{1}{2}}=\begin{pmatrix}Q_{j+\frac{1}{2}}{}^1\\Q_{j+\frac{1}{2}}{}^2\end{pmatrix}, \quad q_j=\begin{pmatrix}\delta\bar{F}_j\\\delta\bar{G}_j\end{pmatrix},$$

we may write, in accordance with (3.9), the variational equations derived from (3.6) as

$$A_{j+\frac{1}{2}}q_{j+1}+B_{j+\frac{1}{2}}q_j+C_j\delta E+Q_{j+\frac{1}{2}}=0, \quad 0\le j\le J-1, \quad (3.10)$$

where

$$A_{j+\frac{1}{2}}=\begin{bmatrix}\dfrac{\partial Q_{j+\frac{1}{2}}{}^1}{\partial\bar{F}_{j+1}} & \dfrac{\partial Q_{j+\frac{1}{2}}{}^1}{\partial\bar{G}_{j+1}}\\[2ex]\dfrac{\partial Q_{j+\frac{1}{2}}{}^2}{\partial\bar{F}_{j+1}} & \dfrac{\partial Q_{j+\frac{1}{2}}{}^2}{\partial\bar{G}_{j+1}}\end{bmatrix}, \quad B_{j+\frac{1}{2}}=\begin{bmatrix}\dfrac{\partial Q_{j+\frac{1}{2}}{}^1}{\partial\bar{F}_j} & \dfrac{\partial Q_{j+\frac{1}{2}}{}^1}{\partial\bar{G}_j}\\[2ex]\dfrac{\partial Q_{j+\frac{1}{2}}{}^2}{\partial\bar{F}_j} & \dfrac{\partial Q_{j+\frac{1}{2}}{}^2}{\partial\bar{G}_j}\end{bmatrix},$$

$$C_j=\begin{bmatrix}\dfrac{\partial Q_{j+\frac{1}{2}}{}^1}{\partial E}\\[2ex]\dfrac{\partial Q_{j+\frac{1}{2}}{}^2}{\partial E}\end{bmatrix}.$$

Since the matrix of the coefficients of Eqs. (3.10) is of the form

$$\begin{array}{c}\\j=0\\1\\2\\\vdots\\J-1\end{array}\begin{array}{c}\begin{array}{ccccccc}q_0 & q_1 & q_2 & q_3 & \cdots & q_{J-1}\ q_J & \delta E\end{array}\\\left[\begin{array}{ccccccc}x & x & & & & & x\\ & x & x & & & & x\\ & & x & x & & & x\\ & & & & & & \\ & & & & x & x & x\end{array}\right]\end{array},$$

we have J equations in $J+2$ unknowns. The two additional conditions which are necessary to solve the equations are given by the boundary condition at $j=0$ and the asymptotic condition at $j=J$.

At $j=0$, $\bar{F}_0$ is given by either of (3.3) when we have chosen $\bar{G}_0=1$ arbitrarily. Then $q_0=0$ and the first equation of (3.10) gives q_1 in terms of δE. Using this relation we eliminate q_1 from the second of (3.10) to give q_2 in terms of δE. The elimination process is continued to the final equation which gives q_J in terms of δE. These equations will be of the form

$$q_j=e_j\delta E+f_j, \quad 0\le j\le J,$$
$$q_0=0. \qquad (3.11)$$

Substituting the first of (3.11) into (3.10) we find recursion relations for the two-vectors e_j and f_j as

$$e_{j+1}=-A_{j+\frac{1}{2}}{}^{-1}(B_{j+\frac{1}{2}}e_j+C_j),$$
$$f_{j+1}=-A_{j+\frac{1}{2}}{}^{-1}(B_{j+\frac{1}{2}}f_j+Q_{j+\frac{1}{2}}). \qquad (3.12)$$

Since $q_0=0$, $e_0=f_0=0$ and we may determine all the e_j, f_j from (3.12) for $0\le j\le J$.

At $j=J$ we write the asymptotic solution (3.5) in difference form as

$$\bar{G}_J=\bar{G}_{J-1}e^{[-\lambda(r_J-r_{J-1})]}. \qquad (3.13)$$

Taking the variation of (3.13) we have

$$\delta\bar{G}_J=e^{[-\lambda(r_J-r_{J-1})]}\big[\delta\bar{G}_{J-1}$$
$$\phantom{\delta\bar{G}_J=}-(r_J-r_{J-1})\bar{G}_{J-1}(d\lambda/dE)\delta E\big], \qquad (3.14)$$

where

$$d\lambda/dE=-E/(1-E^2)^{1/2} \qquad (3.15)$$

from the asymptotic solution.

Now from (3.11) and our definition of q_j we have

$$\delta G_{J-1}=e_{J-1}{}^{(2)}\delta E+f_{J-1}{}^{(2)} \qquad (3.16)$$

and

$$\delta G_J=e_J{}^{(2)}\delta E+f_J{}^{(2)},$$

where the superscript "2" refers to the lower element of the e, f two-vectors. Substituting (3.16) into (3.14) and

---

[10] L. G. Henyey, L. Wilets, K. H. Böhm, R. LeLevier, and R. D. Levee, Astrophys. J. 129, 628 (1959).

[11] L. G. Henyey (private communication to Levee).

solving for E, we arrive at

$$\delta E = \frac{e^{-\lambda(r_J - r_{J-1})} f_{J-1}^{(2)} - f_J^{(2)}}{e_J^{(2)} + [\bar{G}_{J-1}(r_J - r_{J-1})(d\lambda/dE) - e_{J-1}^{(2)}]e^{-\lambda(r_J - r_{J-1})}} . \tag{3.17}$$

The iteration process may be summarized as follows: (1) From the pth approximation to $\bar{F}_j$, $\bar{G}_j$, and E, compute the elements of $A_{j+\frac{1}{2}}$, $B_{j+\frac{1}{2}}$, C_j and $Q_{j+\frac{1}{2}}$ for $0 \leq j \leq J-1$. (2) Using (3.12) compute e_1, e_2, $\cdots$, e_J; f_1, f_2, $\cdots$, f_J using $e_0 = f_0 = 0$. (3) Compute δE by (3.17). (4) Compute the corrections $\delta \bar{F}_1$, $\delta \bar{F}_2$, $\cdots$, $\delta \bar{F}_J$, $\delta \bar{G}_1$, $\delta \bar{G}_2$, $\cdots$, $\delta \bar{G}_J$ from the first of (3.11). (5) Compute the $p+1$st approximations by

$$E^{p+1} = E^p + \delta E^p$$
$$\left. \begin{array}{l} \bar{F}_j{}^{p+1} = \bar{F}_j{}^p + \delta \bar{F}_j{}^p \\ \bar{G}_j{}^{p+1} = \bar{G}_j{}^p + \delta \bar{G}_j{}^p \end{array} \right\} 0 < j \leq J .$$

This process is repeated until all the unknowns satisfy the inequality

$$|\delta x_k{}^p / x_k{}^{p+1}| < T_2, \quad k = 1, 2, \cdots, K$$

and $|\delta E/E| < T_1$ for $x_k > T_3$. For $x_k < T_3$ we do not make a test.

In addition to satisfying the above tolerance tests, we must also have chosen r_J such that the asymptotic solution is indeed valid. To check this we compute

$$\hat{\bar{F}}_{J-1} = \bar{F}_{J-2} e^{-\lambda(r_{J-1} - r_{J-2})}$$
$$\hat{\bar{G}}_{J-1} = \bar{G}_{J-2} e^{-\lambda(r_{J-1} - r_{J-2})}$$

and require that

$$|(\hat{\bar{F}}_{J-1} - \bar{F}_{J-1})/\bar{F}_{J-1}| < T_1$$

and that

$$|(\hat{\bar{G}}_{J-1} - \bar{G}_{J-1})/\bar{G}_{J-1}| < T_1 .$$

If these inequalities are satisfied we are finished. If they are not, we advance J by 10 and resolve the equations. This procedure is repeated until all tests are satisfied.

In order to normalize our solutions we require that

$$N^2 \int_0^\infty r^{\gamma+1}(\bar{F}^2 + \bar{G}^2) dr = 1 = N^2 \int_0^\infty H(r) dr .$$

This quadrature was performed by Bessell's formula

$$\int_0^\infty H(r) dr = \sum_{j=0}^4 C_j(H_j + H_{J-j}) + \sum_{j=5}^{J-5} H_j + \int_{r_J}^\infty H(r) dr$$

where the C_j take on the values

$$C_0{}^1 = 0.32986, \quad C_1{}^1 = 1.32083, \quad C_2{}^1 = 0.76667,$$
$$C_3{}^1 = 1.10139, \quad C_4{}^1 = 0.98125.$$

The final values of the wave functions for the bound state are given by

$$\left. \begin{array}{l} F_j = N r^{\gamma-1} \bar{F}_j \\ G_j = N r^{\gamma-1} \bar{G}_j \end{array} \right\} 0 \leq j \leq J .$$

In the results reported here we have taken $T_1 = 10^{-4}$, $T_2 = 10^{-5}$, $T_3 = 10^{-5}$. The actual iteration error is much smaller since the tests involve comparison with values from the preceding iteration. In fact, since Newton's method doubles the number of significant figures when within the linear range, iteration errors are probably less than 10^{-8}.

B. The Continuum-State Wave Equations

The continuum-state wave equations

$$(\epsilon + 1 + \varphi)f_\kappa - [(dg_\kappa/dr) + (1 + \kappa)(g_\kappa/r)] = 0$$
$$(\epsilon - 1 + \varphi)g_\kappa + [(df_\kappa/dr) + (1 - \kappa)(f_\kappa/r)] = 0 \tag{3.18}$$

constitute an initial value problem since ϵ, the energy of the ejected electron, is determined by the sum of the incident photon energy and the energy of the bound state determined in the previous section.

As in the case of the bound state, it is convenient to make a change of variables here also.

$$f_\kappa = \bar{f}_\kappa r^{\gamma-1}, \quad g_\kappa = \bar{g}_\kappa r^{\gamma-1} .$$

Equations (3.18) then become

$$(\epsilon + 1 + \varphi)\bar{f}_\kappa - [d\bar{g}_\kappa/dr + [(\gamma + \kappa)/r]\bar{g}_\kappa] = 0$$
$$(\epsilon - 1 + \varphi)\bar{g}_\kappa + [d\bar{f}_\kappa/dr + [(\gamma - \kappa)/r]\bar{f}_\kappa] = 0 \tag{3.19}$$

where $\bar{f}_\kappa$ and $\bar{g}_\kappa$ are finite at $r = 0$.

In a manner similar to the bound state we determine at $r = 0$ for a Coulomb potential a/r

$$a\bar{f}_\kappa(0) = (\gamma + \kappa)\bar{g}_\kappa(0) \tag{3.20a}$$

or

$$a\bar{g}_\kappa(0) = -(\gamma - \kappa)\bar{f}_\kappa(0) . \tag{3.20b}$$

Thus $\gamma^2 = \kappa^2 - a^2$ and since Eqs. (3.20) are linear we may again choose $\bar{g}_\kappa(0)$ arbitrarily equal to 1. We then may determine $\bar{f}_\kappa(0)$ from either of (3.20). In practice we use (3.20a) for $\kappa > 0$ and (3.20b) for $\kappa < 0$ to insure the greatest accuracy.

In order to normalize the continuum solution properly, it is necessary to find the asymptotic solution. This is done by matching the solutions of (3.18) with φ not zero to general solutions of (3.18) with φ equal to zero,

and evaluating the asymptotic behavior from the zero-φ solutions beyond the range of the potential.

Let the matching of solutions be done at a point r_0. Let $p^2 = \epsilon^2 - 1$. Then

$$f_\kappa(r_0) = [(\epsilon-1)/pr_0]^{1/2}$$
$$\times [A_+ J_{\kappa-\frac{1}{2}}(pr_0) + A_- J_{-(\kappa-\frac{1}{2})}(pr_0)]$$
$$g_\kappa(r_0) = [(\epsilon+1)/pr_0]^{1/2}$$
$$\times [A_+ J_{\kappa+\frac{1}{2}}(pr_0) - A_- J_{-(\kappa+\frac{1}{2})}(pr_0)]. \quad (3.21)$$

These two equations serve to determine the constants A_+ and A_-. The asymptotic behavior of f_κ and g_κ is then determined by the asymptotic form of the Bessel functions.

$$f_\kappa(r) \sim \left(\frac{2(\epsilon-1)}{\pi}\right)^{1/2} \frac{1}{pr}\left[A_+ \cos\left(pr - \frac{\pi\kappa}{2}\right)\right.$$
$$\left. + A_- \cos\left(pr + \frac{\pi\kappa}{2} - \frac{\pi}{2}\right)\right],$$
$$g_\kappa(r) \sim \left(\frac{2(\epsilon+1)}{\pi}\right)^{1/2} \frac{1}{pr}\left[A_+ \cos\left(pr - \frac{\pi\kappa}{2} - \frac{\pi}{2}\right)\right.$$
$$\left. - A_- \cos\left(pr + \frac{\pi\kappa}{2}\right)\right]. \quad (3.22)$$

The normalization factor A and the phase shift δ_κ are given by

$$A = (A_+^2 + A_-^2)^{1/2},$$
$$\cos\delta_\kappa = A_+/A, \quad (3.23)$$
$$-\sin\delta_\kappa = (-1)^\kappa A_-/A.$$

The asymptotic forms of f_κ and g_κ are then

$$f_\kappa(r) \sim \left(\frac{2(\epsilon-1)}{\pi}\right)^{1/2} \frac{A}{pr} \cos\left(pr - \frac{\kappa\pi}{2} + \delta_\kappa\right),$$
$$g_\kappa(r) \sim \left(\frac{2(\epsilon+1)}{\pi}\right)^{1/2} \frac{A}{pr} \sin\left(pr - \frac{\kappa\pi}{2} + \delta_\kappa\right). \quad (3.24)$$

In using this with a true Coulomb potential, the phase shifts δ_κ will not become constant with increasing r, but rather will continue to increase, behaving like $(a\epsilon/p)\ln 2pr + $constant. This must be taken into account when checking whether the asymptotic form is attained. For potentials that die out more rapidly than the Coulomb potential, the δ_κ's should become constants in r.

The numerical solution of either (3.18) or (3.19) is straightforward except near $r=0$. Because of the singularity exhibited in (3.18) at $r=0$ we use (3.19), but even here we have a starting problem.

Let us write Eqs. (3.19) in the vector notation

$$\omega_\kappa' = A_\kappa \omega_\kappa, \quad (3.25)$$

where ω_κ has components $\bar{f}_\kappa$, $\bar{g}_\kappa$ and where

$$A_\kappa = \begin{bmatrix} -\dfrac{\gamma-\kappa}{r} & -\left(\epsilon-1+\dfrac{a}{r}\right) \\ \left(\epsilon+1+\dfrac{a}{r}\right) & -\dfrac{(\gamma+\kappa)}{r} \end{bmatrix}. \quad (3.26)$$

Consider now the finite difference representation of (3.25) based on the Euler approximation

$$(\omega_{j+1} - \omega_j)/h = A_j \omega_j, \quad j>0, \quad (3.27)$$

where $h = r_{j+1} - r_j = $a constant, and where we have for simplicity dropped the subscript κ. Equation (3.27) is restricted to $j>0$ since the elements of A_j are singular for $j=0$. In practice ω_1 would be determined from ω_0 by a series expansion. Equations (3.27) may be written

$$\omega_{j+1} = (I + hA_j)\omega_j.$$

The first-order error equation will then be

$$\delta\omega_{j+1} = (I + hA_j)\delta\omega_j, \quad (3.28)$$

where we have neglected errors in A_j. Equation (3.28) may be simplified to

$$\delta\omega_{j+1} = B_j \delta\omega_j, \quad (3.29)$$

with

$$B_j = \begin{bmatrix} 1 - \dfrac{h}{jh}(\gamma-\kappa) & -h\left(\epsilon-1+\dfrac{a}{jh}\right) \\ h\left(\epsilon+1+\dfrac{a}{jh}\right) & 1 - \dfrac{h(\gamma+\kappa)}{jh} \end{bmatrix} \quad (3.30)$$

and where we have replaced r by $r_0 + jh = jh$.

If individual errors in ω_j are to remain bounded, we must require that the eigenvalue of the matrix B_j be less than or equal to 1 in absolute value. The eigenvalues of (3.30) are determined from

$$\begin{bmatrix} 1 - \dfrac{(\gamma-\kappa)}{j} - \lambda & -h\left(\epsilon-1+\dfrac{a}{jh}\right) \\ h\left(\epsilon+1+\dfrac{a}{jh}\right) & 1 - \dfrac{(\gamma+\kappa)}{j} - \lambda \end{bmatrix} = 0.$$

The argument holds in the limit of $h \to 0$ which leads to

$$[1 - (\gamma-\kappa)/j - \lambda][1 - (\gamma+\kappa)/j - \lambda] + a^2/j^2 = 0. \quad (3.31)$$

Remembering that $\gamma^2 = \kappa^2 - a^2$ we solve (3.31) to give $\lambda = 1$, $1 - (2\gamma/j)$. Since we require $|\lambda| \leq 1$ we have $-1 \leq 1 - (2\gamma/j) \leq 1$. Now γ and j are always greater than zero and therefore the right-hand inequality is always satisfied. The left-hand inequality will be satisfied if $j > \gamma$. The conclusion is that if we want errors to decrease in the solution of (3.19) by numerical integration, we must begin the integration at a value of

$j \geq \gamma$. The maximum value of γ in our calculations was 20 corresponding to $\kappa = \pm 20$ and it is therefore necessary to use the starting series described below for the first 20 steps. Although the above analysis is applied to the simple Euler method it leads to the same result where applied to the Runge-Kutta method. In fact, it was using the Runge-Kutta method for starting that led to the observations of the error growth and the analysis.[12] It has been pointed out to the authors by J. Scofield[13] that the modified Euler scheme, $\omega_{j+1} = [(I + \frac{1}{2}hA_{j+\frac{1}{2}})/(I - \frac{1}{2}hA_{j+\frac{1}{2}})]\omega_j$ has eigenvalues $\lambda = 1$, $[1 - \gamma/(j+\frac{1}{2})]/[1 + \gamma/(j+\frac{1}{2})]$ in the limit as $h \to 0$. Therefore errors in this scheme will be bounded since $\gamma > 0$.

The power-series solution to (3.19) around the point r_n is of the form

$$\bar{f}(r) = \sum c_i(r - r_n)^i, \quad i = 0, 1, 2, \cdots,$$
$$\bar{g}(r) = \sum b_i(r - r_n)^i, \quad i = 0, 1, 2, \cdots. \quad (3.32)$$

Substituting into (3.19) we arrive at the recursion relations

$$r_n(i+2)b_{i+2} + (i+1)b_{i+1} + (\gamma+\kappa)b_{i+1}$$
$$- [(\epsilon+1)r_n + a]c_{i+1} - (\epsilon+1)c_i = 0,$$
$$r_n(i+2)c_{i+2} + (i+1)c_{i+1} + (\gamma-\kappa)c_{i+1}$$
$$+ [(\epsilon-1)r_n + a]b_{i+1} + (\epsilon-1)b_i = 0,$$

where $c_0 = \bar{f}(r_n)$, $b_0 = \bar{g}(r_n)$. These relations allow the determination of the c_i, b_i for $i > 0$ for successive expansions about $r_n = 0$, $r_n = h$, $r_n = 2h$, $\cdots$, $r_n = jh$. Since we are always expanding about the previous point, $r - r_n = h$.

The series solutions (3.32) and similar equations for the derivatives of $\bar{f}$ and $\bar{g}$ were computed out to $j = JJ$. The series at each j were terminated when the percentage error in f' and g' was less than one part in 10^8. Using the functions and derivatives thus determined, the numerical solution of (3.32) was then continued by the Runge-Kutta method. In the case of a general potential where the series solution is not easily arrived at, we plan using the modified Euler scheme for starting the integration.

At this point in j we switched back to using f and g instead of $\bar{f}$ and $\bar{g}$ so that our numbers would not become too small. In addition it was necessary to add a scale factor, SF, in both f and g in certain cases to keep numbers within machine limits. Using the values

$$f_{JJ} = \bar{f}_{JJ}(SF \cdot r_{JJ})^{\gamma-1}$$
$$g_{JJ} = \bar{g}_{JJ}(SF \cdot r_{JJ})^{\gamma-1}$$
$$f_{JJ}' = \bar{f}_{JJ}'(SF \cdot r_{JJ})^{\gamma-1} + (\gamma-1)f_{JJ}/r_{JJ}$$
$$g_{JJ}' = \bar{g}_{JJ}'(SF \cdot r_{JJ})^{\gamma-1} + (\gamma-1)g_{JJ}/r_{JJ},$$

the numerical integration of (3.32) was continued by the standard Runge-Kutta method.

---

[12] This difficulty had been observed and resolved previously by Levee in a problem in controlled thermonuclear reactions.

[13] J. Scofield (private communication).

Although our analysis in this section indicates that we should take $JJ = 20$, we actually used $JJ = 10$. This allowed small errors to appear in the normalization factors and wave functions for $\kappa > 10$. These errors were of the order of 4% in the normalization factor at $\kappa = 16$. However, the high values of κ contributed very little to the cross sections and the cross sections show no error due to using $JJ = 10$ instead of 20.

We require f and g to be normalized such that

$$f \sim \left(\frac{\epsilon-1}{2\epsilon}\right)^{1/2} \frac{1}{pr} \cos\left(pr - \frac{l\pi}{2} + \delta\right)$$

$$g \sim \left(\frac{\epsilon+1}{2\epsilon}\right)^{1/2} \frac{1}{pr} \sin\left(pr - \frac{l\pi}{2} + \delta\right). \quad (3.33)$$

From (3.23) and (3.33) we then have the following relation for the normalization factor N_1: $N_1 = 2A(\epsilon/\pi)^{1/2}$ where A is determined from (3.21) and the first of (3.23).

The phase δ must now be determined. For a potential which falls off more rapidly than $1/r$ the phase will be given by (3.23) as $\delta = \arctan|A_-/A_+|$, but for the pure Coulomb potential $\delta = \arctan|A_-/A_+| - (a\epsilon/p)\ln 2pr$.

In the program reported here we have computed A at each step of the integration and required that

$$\left|2\frac{A_{j+10} - A_j}{A_{j+10} + A_j}\right| < T_4.$$

It turned out that for the very small T_4 chosen, the integration was always carried out to the predetermined maximum at $r = 120$. At this point the normalizations and phases were determined.

IV. ACCURACY OF THE NUMERICAL CALCULATION

We have seen that we will have all the information needed to specify the properties of S-state photoeffect when we have calculated the quantities $R_\kappa^\pm$ given by Eq. (2.20). We have not discussed how many of these quantities we need to calculate, i.e., the convergence properties of the series in Eqs. (2.24) and (2.27). We follow usual practice, and will judge the convergence by the size of successive $R_\kappa^\pm$. Practical considerations force us to choose a limit for $|\kappa|$ in advance, since the methods employed for calculating functions and organizing the numerical program for machine purposes depend on this choice; in the present paper we consider $|\kappa| \leq 20$.

Then first of all the calculation of a given R_κ requires bound-state radial functions F_κ, G_κ, continuum radial functions f_κ, g_κ, and spherical Bessel functions $j_l(kr)$. Also, in calculating angular distributions we will need the associated Legendre functions $P_l^m(\cos\theta)$, for $m = 0$, 1, 2. The accuracy of the calculations of these *components* of the general program are discussed in separate subsections. We can then estimate the accuracy with which each R_κ has been computed, and the accuracy this implies for the cross sections. And we must also judge

the error which has been made due to the restriction $|\kappa| \leq 20$.

Checks for the component programs will be discussed separately. A number of checks are available for the final results: We can compare with analytic results for low Z and we can compare with numerical results which have previously been obtained for photoelectric cross sections. These comparisons are made in the subsequent sections where we present our results. In all cases the proper agreement was obtained, so that we have full confidence in our numerical program. It should perhaps also be mentioned that with the present program some ten minutes of IBM-7090 time were required to obtain the differential and total cross sections and polarization correlations for a given choice of element and energy; it is expected that further improvements in the program will appreciably reduce this figure.

A. Component Programs

i. Bound-State Wave Functions

The accuracy of the bound-state calculation can be tested for the pure Coulomb potential by comparison with analytic results. It is particularly simple to check the eigenvalue and the normalization of a calculated wave function. The energy levels are obtained with considerable accuracy. However, the normalization coefficient, i.e., the constant which multiplies the known small r dependence, probably gives a better indication of the over-all accuracy of the wave function. For given $h \equiv r_{i+1} - r_i$, the error in mormalization increases with Z. With $h = 0.05$, the smallest value used, the error is negligible for $Z = 26$ or 50 but 0.4% for $Z = 82$ and 0.6% for $Z = 92$. To obtain 1% accuracy in the cross sections for heavy elements we have taken results for $h = 0.1$, 0.075, and 0.05 and extrapolated to $h = 0$. [Note: It has since been established that these small errors result from a minor error in programming; once this is corrected, the error in bound-state normalizations becomes completely negligible.]

ii. Continuum-State Wave Functions

The two parameters of a continuum-state solution which are easily compared with the analytical results of the pure Coulomb potential are normalization and

TABLE I. Accuracy of continuum normalizations.

Energy (MeV)	κ +1 (%)	+5 (%)	+9 (%)	+15 (%)
Low Z 0.354	0.01	0.02	0.4	4.0
1.131	0.01	0.03	0.4	4.5
High Z 0.200	0.5	0.7	1.0	5.0
0.354	0.1	0.2	0.5	4.5
0.600	0.07	0.10	0.45	4.4
1.131	0.03	0.05	0.4	4.2
1.5	0.02	0.03	0.3	4.0
2.0	0.2	0.2	0.4	4.2

TABLE II. Accuracy of phase shifts; errors in radians and percent.

Energy (MeV)	κ +1	+5	+9	+15
Low Z 0.354	0.0004(2%)	0.0004(0.1%)	0.0005(0.1%)	0.0009(0.1%)
1.131	0.0015(10%)	0.0016(0.5%)	0.0014(0.3%)	0.0014(0.2%)
High Z 0.200	0.0035(∞)	0.0054(0.3%)	0.0001(0.0%)	0.0021(0.1%)
0.354	0.0030(1.5%)	0.0005(0.0%)	0.0019(0.1%)	0.0034(0.2%)
0.600	0.0007(0.2%)	0.0001(0.0%)	0.0006(0.1%)	0.0012(0.1%)
1.131	0.0011(0.3%)	0.0009(0.1%)	0.0011(0.1%)	0.0014(0.1%)

phase. The accuracy of the normalizations calculated with $h = 0.05$ for some typical partial waves in low-Z (26) and high-Z (82 and 84) elements are shown for various energies in Table I. The errors in the higher partial waves are nearly independent of energy (away from threshold) and Z, but increase rapidly with κ. These arise from the use of the same switching point $JJ = 10$ from power series to numerical integration for all κ. Except at the highest energy (2 MeV), the errors are not sensitive to choices of h in the range from 0.05 to 0.1. The error in normalization also increases rapidly as the threshold energy is approached. This type of error is insensitive to h and may be connected with the very long periods of low-energy continuum states. In Table II we give the analogous errors in phase shifts, expressed both in radians and in percent.

iii. Spherical Bessel Functions

The spherical Bessel functions j_l, $0 \leq l \leq 20$, were computed by the method of Corbató and Uretsky[14] and were checked against the NBS Tables[15] for selected values of l. The errors were less than one part in 10^6.

iv. Legendre Polynomials

The Legendre and associated Legendre functions were computed in double precision arithmetic directly from the polynomials given by Tallquist.[16] These were compared with double precision values computed from the recursion relations and found to agree to at least one part in 10^{12}. Rough comparisons can be made to the tables of Mursi[17] and NBS.[18]

B. The Main Program

i. Partial-Wave Integrals R_κ

The errors in an R_κ are due first to the errors of the component programs and second to the errors of the

[14] F. J. Corbató and J. L. Uretsky, J. Assoc. Comp. Mach. 6, 366 (1959).

[15] National Bureau of Standards, Tables of Spherical Bessel Functions (Columbia University Press, New York, 1947), Vols. I and II.

[16] H. J. Tallquist, Acta Soc. Sci. Fennicæ, Nova Series A, Tome II, No. 4 (1936); Tome II, No. 11 (1938).

[17] Z. Mursi, Tables of Legendre Associated Functions (E. and R. Schindler, Cairo, 1941).

[18] National Bureau of Standards, Tables of Associated Legendre Functions (Columbia University Press, New York, 1945).

TABLE III. Regions contributing to partial-wave integrals.

Z	Energy (MeV) κ	+1	+5	+9	+15
26	0.354	84	80	108	(does not contribute)
	1.131	58.5	63	78.5	89.5
50	0.354	41	45	50	(does not contribute)
92	0.208	19	28.5	35	(does not contribute)
84	0.354	20	26	31.5	(does not contribute)
	1.131	22	25	27	31
82	1.1368	21.5	23	27	28.5
	2.0	19.5	25	26	27
	2.754	22.5	24.5	25	25.5

integration procedures. The errors in integration arise from the choice of h and r_{max}, the upper limit of the integration.

Table III summarizes, for representative parameters, the distance in r which it was necessary to integrate to hopefully reduce the residual contribution to less than one part in 10^6. The needed distance increases slowly with increasing κ; in heavy elements it is nearly independent of energy and is determined by the decreasing exponential of the bound-state wave function. Since this exponential scales as Z the required distance greatly increases as Z decreases. In light elements this has the consequence that an energy dependence persists in the energy range of concern, and the rapid oscillations of a high-energy continuum-state work to reduce the needed distance.[19] Since such a stringent criterion was applied in the table, it is possible to obtain satisfactory results from the present calculation for a Z as low as 10 or 13, even with the restriction $r_{max} \leq 120$ required in the machine program.

The error in integration arising from the choice of h can be estimated by noting the change in the values of R_κ resulting from changes in h and subtracting out the portion of this which is due to change in component programs with h. As already noted, up to 1.5 MeV, the only component program which is sensitive to choices of h in the range 0.05–0.10 is the bound-state wave func-

TABLE IV. Number of κ's needed for accuracy to one part in 10^n.

E n	1	2	3	4	5	6
0.140	2	3	4	4	5	5
0.200	3	4	5	6	7	8
0.279	3	4	6	7	8	9
0.354	4	5	7	9	10	12
0.400	4	6	8	9	11	13
0.662	5	8	10	13	14	
1.131	7	12	15			
1.1368	8	13	16			
2.0	11	≈ 17				
2.754	14					

---

[19] It should be noted that the distance required for very high accuracy has a different dependence on parameters from the distance which characterizes the main region of the integrand. It is the latter distance which is discussed in the various analytic approximations.

tion. When the estimated error from this source is subtracted, the residual error to be attributed to error from h in integration is generally small and, with one exception,[20] completely independent of κ. The typical error begins to increase at higher energies: the difference between R_κ of $h=0.05$ and 0.10, still negligible at 662 keV, is about 0.4% at 1.131 MeV, both for $Z=26$ and 82, and 1.5% at 1.5 MeV.

ii. Number of κ's Contributing to Cross Section

The number of κ's needed to determine the total cross section to any desired accuracy increases with energy, but it is almost independent of Z. One or two more κ's are needed to obtain the same accuracy for $Z=26$ as for $Z=84$. In Table IV we summarize as a function of energy (for heavy elements) the number of κ's needed to obtain an accuracy of one part in 10^n. The restriction to $|\kappa| < 20$ results in a limitation to energies below about 2 MeV if it is desired to obtain the total cross section to 1%.

TABLE V. Estimates of total error in numerical calculation.

	Energy	Error in σ_{total} (%)
Low Z	0.354	0.2
	1.131	0.6
High Z	0.200	1.1
	0.354	0.5
	0.600	0.5
	1.131	0.8
	1.368	0.8
	2.00	2.0

iii. Estimate of Total Error in Cross Sections

We assume that a fit is made to the results for different h and extrapolated to $h=0$, and we assume that, in agreement with our analysis, this renders errors associated with h (bound-state normalization, integration, etc.) negligible, i.e. 0.1%. Then the error in R_κ is dominated by the error in the continuum wave function. From this estimate of the error in each R_κ, and from the information just presented on the contribution of each κ to the cross section, we can get an estimate of the total error of the cross section. Some rough estimates of this kind are summarized in Table V. The main conclusion is that the present calculation obtains total cross sections accurate to 0.8% in the energy range from 300 to 1400 keV; the accuracy decreases rapidly toward threshold and at high energies.

V. TOTAL CROSS SECTIONS

Theoretical predictions for the total K-shell photo-electric-effect cross section have been based on four

---

[20] The exception is for $\kappa=1$, for which R_κ changes by as much as 0.5% between $h=0.05$ and 0.10.

TABLE VI. Total cross sections for $Z=13, 26, 50, 84$, in barns.

Z	13	26		50		84	
E (MeV)	This work	This work	Hulme et al.	This work	Hulme et al.	This work	Hulme et al.
0.3543	0.01543	0.3885	0.39	7.06	7.1	60.6	60.2
0.662	0.00289	0.0754	⋯	1.455	⋯	13.87	⋯
1.131	0.00091	0.0237	0.023	0.462	0.46	4.54	4.61
1.5	0.00054	0.0140	⋯	0.271	⋯	2.65	⋯
2.0	0.00033	0.0086	⋯	0.164	⋯	1.57	⋯

TABLE VIII. Comparison of total cross sections (in barns) for $Z=82$, from the NBS tables, an extrapolation of Pratt, and the present calculation.

E (MeV)	NBS	Extrapolation	Present calculation
1.131	4.37	4.07	4.10
1.332	3.24	3.03	2.99
1.5	2.65	2.49	2.39
2.0	1.8	1.56	1.42

main calculations: (1) The exact nonrelativistic solution of the problem, usually associated with Stobbe,[21] (2) Sauter's relativistic calculation,[6] valid to lowest order in $Z\alpha/\beta$, (3) numerical calculations of Hulme et al.[22] for a few selected energies and elements, (4) the high-energy limit of the relativistic problem for arbitrary Z as given by Hall.[23] Extrapolation procedures, based on these four results, can be used to estimate the cross section for arbitrary Z and energy; tables of these predictions have been given by Grodstein[24] (NBS tables). Experimental results have generally yielded satisfactory agreement with these tables.

Since 1955 there has been substantial improvement in all four of these calculations, and one of them has actually been found to contain an error. Namely, although Hall's expression for the high-energy limit in the form of a double integral is correct, the analytic formula with which he approximated the integral is not, and overestimates the cross section by a factor of two in heavy elements. The exact high-energy limit was obtained numerically by Pratt[7] and later confirmed by Hall[25]; as already noted, Eq. (2.7) gives a fairly good

analytic representation. It is then at first hard to understand why the extrapolation between Sauter and Hall is in good agreement with Hulme. The work of Gavrila[26] and Nagel,[27] who extended Sauter's result to next order in $(Z\alpha/\beta)$, explains the puzzle. Hall's error essentially involved omission of the factor $(-4\pi a/15)$ in Eq. (2.7), but the energy dependence of this term is such that it is large only at very high energies. [Recently, a complicated analytical expression for still another order in $Z\alpha/\beta$ has been given by Gorshkov and Mikhailov.[28]]

K-shell photoeffect at threshold has been calculated for the relativistic problem, both analytically and numerically, by Nagel and Olsson.[5] In the low-energy region screening effects are expected to be important, however, and this has recently been examined in the nonrelativistic problem by Cooper.[29] Since, as already noted, the numerical techniques of the present paper require modification at low energies, we will not discuss this energy region further.

The numerical calculations of Hulme et al. provided the reference points which Sauter-Stobbe and Sauter-Hall extrapolations are forced to fit. The accuracy of Grodstein's predictions for intermediate energies rests almost entirely on the accuracy of these numerical results obtained for 0.3543 and 1.131 MeV, estimated at 4% for heavy elements and 8% for lighter elements. Since this is the main energy region of experimental interest, it is important to verify and extend these

TABLE VII. Total cross sections for $Z=82, 92$, in barns.

E (MeV)	$Z=82$ This work	HNO	NBS	E (MeV)	$Z=92$ This work	HNO	NBS
0.120	⋯	921	950				
0.200	239	241	236	0.132	⋯	1026	1100
0.300	84.0	83.6	80.2	0.140	⋯	887	942
0.400	40.7	40.5	40.4	0.208	319	324	334
0.500	23.7	23.7	23.1	0.279	155	154	155
0.600	15.6	15.5	15.3	0.412	59.9	59.5	59.8
0.662	12.5	⋯	12.4	0.662	20.4	20.2	20.7
0.900	6.49	⋯	6.68	0.900	10.7	⋯	11.2
1.131	4.10	⋯	4.37	1.131	6.78	⋯	7.38
1.332	2.99	⋯	3.24	1.332	4.93	⋯	5.5
1.5	2.39	⋯	2.65	1.5	3.95	⋯	4.5
2.0	1.42	⋯	1.8	2.0	2.33	⋯	2.9

TABLE IX. Comparison with experimental results (see Refs. 32–34) for K-shell total cross sections (in barns).

Experimenter	Element	Energy (keV)	Experimental result	Present theory
Seeman	Pb	511	23.4 ±0.7	22.5
Missoni	Au	662	10.2 ±0.3	10.5
Hultberg and Stockendal	U	1173	7.2 ±0.5	6.32
Hultberg and Stockendal	U	1332	5.4 ±0.3	4.93
Bleeker, Goudsmit and De Vries	Pb	1332	3.24±0.13	2.99

[21] M. Stobbe, Ann. Physik 7, 661 (1930).

[22] H. R. Hulme, J. McDougall, R. A. Buckingham, and R. H. Fowler, Proc. Roy. Soc. (London) A149, 131 (1935).

[23] H. Hall, Rev. Mod. Phys. 8, 358 (1936).

[24] G. W. Grodstein, U. S. Department of Commerce, National Bureau of Standards Circular 583 (U. S. Government Printing Office, Washington, D. C., 1957); see also R. T. McGinnies, NBS Supplement to Circular 583 (1959).

[25] H. Hall, University of California, Lawrence Radiation Laboratory Report UCRL 5947-T (unpublished).

[26] M. Gavrila, Phys. Rev. 113, 514 (1959).

[27] B. Nagel, Arkiv Fysik 18, 1 (1960).

[28] V. G. Gorshkov and A. I. Mikhailov, Zh. Eksperim. i Teor. Fiz. 43, 991 (1962) [English transl.: Soviet Phys.—JETP 16, 701 (1963)].

[29] J. W. Cooper, Phys. Rev. 128, 681 (1962).

TABLE X. K-shell angular distributions for $Z=13, 26, 50, 84$ in barns/steradian (when multiplied by indicated scale factor and by 1490).

Z	13		26		50			84		
E (keV)	354	662	354	662	354	662	1131	354	662	1131
θ \ Scale	10^{-6}	10^{-6}	10^{-4}	10^{-5}	10^{-3}	10^{-3}	10^{-4}	10^{-2}	10^{-3}	10^{-3}
0			0.0028		0.0155	0.033	0.4		0.79	0.96
5	1.0	0.5	0.19	1.4	0.280	0.22	2.0	0.14	1.91	1.98
10	2.8	1.4	0.62	3.6	0.92	0.59	4.3	0.43	3.93	3.40
15	4.1	1.7	1.04	4.4	1.58	0.79	4.3	0.78	5.20	3.40
20	4.9	1.6	1.27	4.1	2.00	0.76	2.8	1.06	5.50	2.47
25	5.3	1.3	1.28	3.3	2.10	0.598	1.6	1.23	4.99	1.62
30	4.9	0.9	1.15	2.3	1.95	0.435	1.02	1.26	3.98	1.07
35	3.9	0.58	0.95	1.50	1.67	0.306	0.67	1.20	2.98	0.71
40	2.9	0.37	0.746	1.00	1.36	0.211	0.42	1.08	2.22	0.47
45	2.2	0.26	0.567	0.71	1.07	0.144	0.27	0.93	1.64	0.33
50	1.65	0.17	0.422	0.48	0.820	0.098	0.18	0.78	1.19	0.23
55	1.20	0.11	0.311	0.30	0.621	0.069	0.13	0.64	0.89	0.168
60	0.86	0.08	0.228	0.21	0.468	0.049	0.095	0.51	0.66	0.125
65	0.63	0.06	0.168	0.16	0.351	0.035	0.069	0.41	0.49	0.097
70	0.46	0.04	0.123	0.116	0.264	0.026	0.051	0.33	0.37	0.076
75	0.34	0.028	0.091	0.077	0.199	0.019	0.039	0.26	0.29	0.058
80	0.26	0.020	0.067	0.056	0.150	0.0142	0.031	0.21	0.23	0.046
85	0.19	0.016	0.050		0.113	0.0109	0.024	0.17	0.17	0.038
90	0.140	0.012	0.037		0.086	0.0083	0.019	0.13	0.14	0.032
95	0.101		0.028		0.066	0.0064				
100	0.076		0.021		0.051	0.0050				
105	0.057		0.0158		0.039	0.0040				
110	0.042		0.0120		0.030	0.0032				
115	0.033		0.0091		0.024	0.0026				
120	0.027		0.0069		0.019	0.0020				
125	0.020		0.0052		0.015	0.0017				

Z	13			26			50		84	
E (keV)	1131	1500	2000	1131	1500	2000	1500	2000	1500	2000
θ \ Scale	10^{-6}	10^{-6}	10^{-6}	10^{-5}	10^{-5}	10^{-5}	10^{-4}	10^{-4}	10^{-3}	10^{-3}
0				0.06	0.05	0.034	0.4	0.36	1.0	1.0
5	0.42	0.4	0.3	1.0	1.0	0.9	2.0	1.8	2.0	1.9
10	0.95	0.79	0.6	2.4	2.0	1.6	3.7	3.0	3.0	2.6
15	0.90	0.63	0.43	2.36	1.60	1.04	2.9	1.87	2.43	1.6
20	0.58	0.31	0.16	1.50	0.80	0.41	1.5	0.76	1.41	0.72
25	0.33	0.15	0.08	0.83	0.39	0.19	0.78	0.37	0.81	0.39
30	0.195	0.09	0.05	0.50	0.24	0.126	0.49	0.24	0.51	0.24
35	0.119	0.061	0.030	0.33	0.17	0.079	0.32	0.15	0.32	0.146
40	0.075	0.034	0.015	0.205	0.091	0.040	0.19	0.086	0.21	0.099
45	0.048	0.019	0.100	0.122	0.053	0.024	0.119	0.056	0.15	0.071
50	0.031	0.014	0.008	0.081		0.014	0.085	0.043	0.105	0.047
55	0.020	0.011		0.060			0.064	0.030	0.075	0.034
60	0.015	0.007					0.045	0.021	0.058	0.030
65	0.012						0.032	0.015	0.047	0.023
70	0.008						0.025	0.012	0.036	0.016

calculated points, and this is the purpose of the present section.

While the present work was in progress a new numerical calculation was reported by Hultberg, Nagel, and Olsson (HNO).[2] Like the work of Hulme et al., the method used applies only to the pure Coulomb potential; HNO treated two heavy elements in the energy range 0.120–0.662 MeV. Moderately good agreement was obtained with the values derived from the NBS tables, confirming the low-energy high-Z point of Hulme et al.[30]

The K-shell total cross sections obtained in the present numerical calculations are summarized in Tables VI and VII. The Z's of Table VI corresponds to those of

---

[30] It should also be noted that in principle, another series of photoeffect total cross sections is available in the numerical calculations on the coherent scattering of photons from K-shell electrons carried out by Brown and collaborators: G. E. Brown, R. E.

Peierls, and J. B. Woodward, Proc. Roy. Soc. (London) A227, 51 (1954); S. Brenner, G. E. Brown, and J. B. Woodward, ibid. A227, 59 (1954); G. E. Brown and D. F. Mayers, ibid. A234, 387 (1955); A242, 89 (1957). As the authors note, the photoeffect cross sections can be obtained from the imaginary part of the scattering amplitude in the forward direction for the coherent process, and results are presented for Hg at photon energies of 0.32, 0.64, 1.28, and 2.56 (all in units of mc^2). A similar calculation was later reported by H. Cornille and M. Chapdelaine, Nuovo Cimento 14, 1386 (1959) for photons of energy 5.12 mc^2 on Hg. Unfortunately, results of these papers pertaining to the photoeffect are not presented as cross sections. We do not wish to now enter into a detailed discussion, but if our interpretation of these results is correct they are in fair accord with our numerical work and the highest energy results show the suppression from previous values reported here.

TABLE XI. K-shell angular distributions for $Z=82, 92$ in barns/steradian (when multiplied by indicated scale factor and by 1490).

Z	82						92			
E (keV)	200	300	400	500	600	662	208	279	412	662
θ \ Scale	10^{-2}	10^{-2}	10^{-2}	10^{-2}	10^{-3}	10^{-3}	10^{-2}	10^{-2}	10^{-2}	10^{-2}
0	0.0006		0.0289	0.0414	0.523	0.577	0.00030	0.0147	0.052	0.104
5	0.132	0.2	0.135	0.143	1.51	1.55	0.122	0.139	0.175	0.228
10	0.499	0.5	0.397	0.376	3.63	3.56	0.47	0.479	0.484	0.489
15	1.02	0.8	0.688	0.600	5.33	4.97	0.98	0.94	0.85	0.690
20	1.61	1.1	0.900	0.717	5.82	5.16	1.57	1.42	1.13	0.740
25	2.16	1.36	0.987	0.717	5.34	4.50	2.16	1.83	1.27	0.673
30	2.59	1.53	0.964	0.642	4.43	3.58	2.69	2.10	1.28	0.577
35	2.88	1.54	0.871	0.536	3.47	2.71	3.10	2.23	1.19	0.437
40	3.02	1.44	0.746	0.428	2.63	2.00	3.37	2.23	1.05	0.332
45	3.02	1.28	0.616	0.333	1.96	1.46	3.50	2.12	0.89	0.250
50	2.91	1.10	0.497	0.255	1.45	1.06	3.50	1.96	0.74	0.187
55	2.72	0.93	0.395	0.194	1.07	0.78	3.40	1.76	0.60	0.140
60	2.48	0.78	0.311	0.148	0.80	0.576	3.22	1.54	0.49	0.106
65	2.22	0.64	0.244	0.112	0.60	0.431	2.98	1.33	0.39	0.080
70	1.96	0.53	0.190	0.086	0.455	0.327	2.72	1.14	0.310	0.062
75	1.71	0.43	0.149	0.066	0.348	0.250	2.45	0.96	0.247	0.048
80	1.47	0.35	0.117	0.051	0.269	0.193	2.18	0.81	0.197	0.038
85	1.26	0.28	0.092	0.040	0.209	0.151	1.93	0.68	0.158	0.030
90	1.07	0.23	0.073	0.031	0.166	0.120	1.69	0.57	0.127	0.024
95	0.91	0.183	0.058	0.025	0.133	0.097	1.47	0.47	0.103	0.0196
100	0.766	0.148	0.047	0.0200	0.108	0.079	1.27	0.39	0.083	0.0161
105	0.644	0.121	0.038	0.0163	0.088	0.064	1.10	0.33	0.068	0.0134
110	0.54	0.101	0.031	0.0134	0.073	0.054	0.94	0.27	0.057	0.0113
115	0.45	0.083	0.026	0.0111	0.062	0.046	0.81	0.230	0.048	0.0098
120	0.38	0.068	0.021	0.0095	0.053	0.039	0.69	0.195	0.041	0.0085
125	0.31	0.056	0.018	0.0082	0.046	0.034	0.59	0.166	0.036	0.0075

Z	82					92				
E (keV)	900	1131	1332	1500	2000	900	1131	1332	1500	2000
θ \ Scale	10^{-3}	10^{-3}	10^{-3}	10^{-3}	10^{-3}	10^{-3}	10^{-3}	10^{-3}	10^{-3}	10^{-3}
0	0.75	0.84	0.90	0.90	0.87	1.37	1.56	1.68	1.7	1.68
5	1.71	1.79	1.84	1.8	1.75	2.62	2.82	2.9	2.9	2.9
10	3.34	3.12	2.94	2.76	2.3	4.81	4.63	4.42	4.2	3.6
15	3.89	3.11	2.57	2.22	1.4	5.68	4.67	3.93	3.4	2.25
20	3.32	2.24	1.63	1.27	0.65	5.04	3.51	2.59	2.04	1.06
25	2.46	1.46	0.98	0.73	0.35	3.88	2.39	1.63	1.22	0.59
30	1.73	0.96	0.62	0.46	0.22	2.83	1.61	1.05	0.77	0.36
35	1.20	0.64	0.402	0.290	0.131	2.01	1.08	0.68	0.49	0.217
40	0.82	0.423	0.264	0.189	0.088	1.42	0.74	0.46	0.33	0.153
45	0.57	0.291	0.183	0.133	0.063	1.01	0.52	0.33	0.236	0.111
50	0.41	0.207	0.129	0.093	0.042	0.73	0.37	0.231	0.166	0.072
55	0.294	0.148	0.092	0.066	0.030	0.54	0.27	0.166	0.118	0.053
60	0.216	0.110	0.070	0.051	0.026	0.40	0.202	0.129	0.093	0.048
65	0.164	0.085	0.056	0.042	0.020	0.31	0.160	0.104	0.077	0.037
70	0.126	0.066	0.042	0.031	0.014	0.24	0.125	0.080	0.059	0.025
75	0.096	0.051				0.185	0.096	0.061		
80	0.075	0.040				0.146	0.077	0.051		
85	0.061	0.033				0.119	0.065	0.044		
90	0.050	0.028				0.098	0.054	0.035		

Hulme et al. and those of Table VII to HNO; in each case the appropriate comparisons with earlier work are made. The first striking feature is the excellent agreement, far better than the accuracy which had been claimed, with the calculations of Hulme et al. This means that interpolations, such as Grodstein's, based on the Hulme values would be expected to be good and need no major revision in this energy range (however, see below). The errors which remain are of the same magnitude as screening effects; such effects must be included before the change in the cross section from the Hulme values is significant. Agreement with the HNO results is also excellent, and within the estimated error of the present calculation. The first result of this section is then the establishment of the accuracy of the values of Hulme et al.

In Table VII we have also given the corresponding cross section as obtained in the NBS tables.[31] The com-

[31] Since the NBS values are for total absorption cross sections, the contribution from higher shells is removed by dividing out the simple multiplicative factor which Grodstein used to put it in. Another smaller correction is also needed to obtain a K-shell cross section without screening.
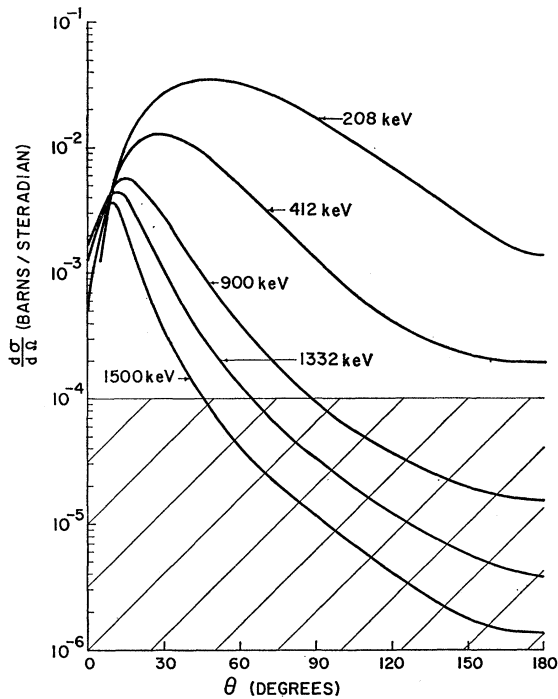
FIG. 1. K-shell angular distributions for U in barns/steradian. The small cross sections in the shaded region of the graph are of low accuracy.

accord with the NBS tables, which again says that the experimental results above 1 MeV are higher than the theoretical values of the present calculation.

The second result of this section is then the finding of significantly lower cross sections in the energy region above 1 MeV than are given in the NBS tables or in two recent experiments. We have previously outlined the evidence for the accuracy of the present calculations. If these arguments are correct we see no theoretical explanation for the discrepancy. It is true that screening effects will modify the pure Coulomb calculations, but for the K shell such corrections are expected to be only 1–2%, and in the wrong direction.

TABLE XII. Comparison of angular distributions with HNO results, normalized to agree with this work at the underlined angles.

E(keV)	208		279		412		662	
θ	This work	HNO	This work	HNO	This work	HNO	This work	HNO
0			0.01		0.05	0.05	0.10	0.13
5	0.12	0.13	0.14	0.17	0.18	0.18	0.23	0.27
10	0.47	0.53	0.48	0.51	0.48	0.48	0.49	0.49
15	0.98	0.97	0.94	0.94	0.85	0.77	0.69	0.68
20	1.57	1.50	1.42	1.38	1.13	1.14	0.74	0.74
25	2.16	2.17	1.83	1.83	1.27	1.27	0.67	0.67
30	2.69	2.73	2.10	2.10	1.28	1.28	0.56	0.56
35	3.10	3.13	2.23	2.23	1.19	1.18	0.44	0.44
40	3.37	3.37	2.23	2.21	1.05	1.04	0.33	0.33
45	3.50	3.47	2.12	2.10	0.89	0.88	0.25	0.25
50	3.50	3.50	1.96	1.95	0.74	0.73	0.19	0.19
55	3.40	3.43	1.76	1.76	0.60	0.61	0.14	0.14
60	3.22	3.23	1.54	1.53	0.49	0.49	0.11	0.11
65	2.98	3.00	1.33	1.34	0.39	0.39	0.08	0.08
70	2.72	2.77	1.14	1.13	0.31	0.30	0.06	0.06
75	2.45	2.47	0.96	0.96	0.25	0.24	0.05	0.05
80	2.18	2.20	0.81	0.81	0.20	0.20	0.04	0.04
85	1.93	1.93	0.68	0.68	0.16	0.16	0.03	0.03
90	1.69	1.70	0.57	0.57	0.13	0.12		
95	1.47	1.47	0.47	0.47	0.10	0.10		
100	1.27	1.27	0.39	0.40	0.08	0.09		
105	1.10	1.10	0.33	0.34	0.07	0.07		
110	0.94	0.93	0.27	0.28	0.06	0.06		
115	0.81	0.80	0.23	0.23	0.05	0.05		
120	0.69	0.67	0.20	0.19				
125	0.59	0.50	0.17	0.17				

parison is rather surprising; even in the 1-MeV region, the present results are 5–10% lower than corresponding interpolations from the NBS tables. It is hard to understand this, since the present results agree with Hulme et al. and the NBS tables are based on Hulme et al. By 2 MeV, the difference has reached 25%. Further proof that this difference is real is provided by a new calculation[32] which HNO have undertaken to check our results; it appears that they have obtained complete agreement with our cross section for $Z=92$ at 1.332 MeV.

A comparison with the extrapolation formula of Pratt[7] is given in Table VIII for $Z=82$. This formula, which is exact at very high energies and exact for light elements at all energies, is in good agreement with the Hulme values and so also with the present calculation in the 1-MeV range. However Table VIII suggests that the very close agreement at 1 MeV is misleading, since for the higher energy of 2 MeV the two differ by 10%.

The recent experimental measurements[33–36] of the total cross section from the K shell are given in Table IX.[37] These results were all reported as in good

[32] S. Hultberg (private communication). We should like to thank Dr. Hultberg for undertaking this calculation and for communicating its results prior to publication.

[33] K. W. Seeman, Bull. Am. Phys. Soc. 1, 198 (1956).

[34] S. Hultberg and R. Stockendal, Arkiv Fysik 15, 355 (1959).

[35] E. J. Bleeker, P. F. A. Goudsmit, and C. DeVries, Nucl. Phys. 29, 452 (1962).

[36] G. Missoni (to be published).

[37] One should also note the measurement by Bleeker, Goudsmit, and DeVries of the ratio $\sigma(2.754)/\sigma(1.368)$ in Pb. A similar ratio

was obtained earlier by G. R. Bishop, C. H. Collie, H. Halban, A. Hedgran, K. Siegbahn, S. duToit and R. Wilson, Phys. Rev. 80, 211 (1950); an early result for $\sigma(2.62)$ in Pb is given by G. D. Latyshev, Rev. Mod. Phys. 19, 132 (1947). See also the total photoelectric absorption cross-section measurements of W. F. Titus, Phys. Rev. 115, 351 (1959), at 662 keV in a series of elements, and of B. I. Deutch and F. R. Metzger, ibid. 122, 848 (1961) at 279 keV in Tl. Particularly interesting for this paper are total absorption measurements at 2.62 MeV in various elements by I. E. Dayton, Phys. Rev. 89, 544 (1953) and W. F. Titus (to be published), which lie appreciably below the earlier theories.

TABLE XIII. Ratio of experiment to theory for angular distributions in U, both distributions normalized to unity at the underlined angles.

Angle\Experimenter Energy (keV)	Sujkowski 279	Hultberg 412	Hultberg 662	Hultberg 1332
0°	6.2	2.2	0.89	0.71
15°	0.95	0.84	1.00	1.00
30°	1.00	1.00	1.04	1.28
45°	1.05	1.10	1.32	0.87
60°	0.94	1.33	1.46	0.91
75°	0.92	1.58	1.68	0.67
90°	0.98	1.90	1.69	0.00

VI. ANGULAR DISTRIBUTIONS

Until quite recently the only theoretical result for the angular distribution of relativistic K-shell photoeffect was that of Sauter,[6] Eq. (2.5), and there was no experimental information. When corrections of relative $O(a)$ were computed by Banerjee,[38] Gavrila,[26] and Nagel[27] it was found that they did not significantly change the predicted angular distributions, including the prediction of a vanishing cross section in the forward direction. On the other hand, the experiments of Hultberg[39–41] indicated some striking deviations from the Sauter distribution: A nonvanishing forward cross section, a shifting of the maximum in the cross section toward *larger* angles, and a tendency of the cross section to hold up at large angles. We shall return to the theoretical discussion of these matters following the presentation of our numerical calculations and their comparison with HNO and experiment.

The K-shell angular distributions obtained in the present numerical calculations are summarized in Tables X and XI. We present these results in some detail, despite their limited accuracy, since they do display the significant deviations from the Sauter distribution and so provide more nearly correct predictions. The very small large-angle cross sections are not tabulated. For qualitative purposes we also show in Fig. 1 the $Z=92$ distributions for several energies. Forward scattering increases with increasing energy, the maximum moves in, and backward scattering remains finite but decreases with increasing energy.

For the lower energies we may again compare these results with those of HNO which become available (although they have not been published) in the course of the present calculation. The comparison for U is given in Table XII, where the HNO values, which are normalized to unity at the angle of maximum emission, are read from their graphs and normalized to agree with

[38] H. Banerjee, Nuovo Cimento 10, 863 (1958).
[39] A. Hedgran and S. Hultberg, Phys. Rev. 94, 498 (1954).
[40] S. Hultberg, Arkiv Fysik 9, 245 (1955).
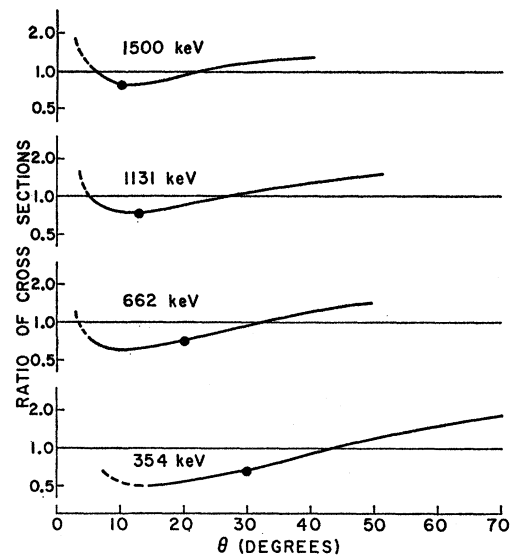[41] S. Hultberg, Arkiv Fysik 15, 307 (1959).

FIG. 2. Comparison with the Sauter angular distribution from $Z=84$ for a series of energies. The ratio R of the present distribution to the Sauter distribution is plotted, where both distributions have been normalized to their respective total cross sections. The approximate angles of maximum emission are marked.

our absolute results at the underlined angles. The two calculations are in good agreement.

Experimental results for K-shell angular distributions have been obtained for uranium by Hultberg[39] (412, 662, and 1332 keV) and by Sujkowski[40] (279 keV); no other true K-shell distributions are known to us, excepting the early work of Hultberg.[37–38] In Table XIII we give, for a few selected angles, the ratio of experiment to theory. The experimental results are available at quite fine angular intervals, and the 279- and 662-keV cases have elsewhere[2,42] been compared with the HNO predictions in graphical form. Except at forward angles the 279-keV result of Sujkowski seems to be in good agreement with theory, and it should be noted that at this low energy the forward cross section is very small. The higher energy data of Hultberg shows more marked deviations from theory; now that fairly good theoretical estimates are available, further experimental data in this energy region would be desirable. Note that at higher energies theory predicts a *larger* forward cross section than was observed. [Angular distributions for Au at 412 keV in the range 20°–90° have now been obtained by Bergkrist and Hultberg[43] in excellent agreement with theory.]

Let us next compare these new theoretical results with the much-used Sauter distribution. This has been done for a series of energies in Fig. 2. What is plotted is the ratio R of the present distribution to the Sauter distribution, with both distributions normalized to their respective total cross section $[(d\sigma/d\Omega)/\sigma]$. Thus, the

[42] Z. Sujkowski, Arkiv Fysik 20, 269 (1961).
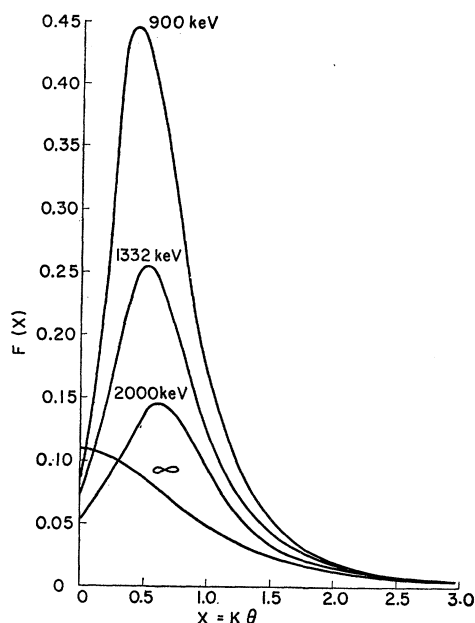[43] K. Bergkvist and S. Hultberg, Arkiv Fysik (to be published).

FIG. 3. High-energy behavior of angular distribution. $F(x)$ $=(4e^2a^5\epsilon)^{-1}(d\sigma/d\Omega)$ is plotted against $x=k\theta$ for $Z=82$ at three energies and compared with its form in the high-energy limit.

straight line $R=1$ corresponds to the Sauter distribution; an angular region in which $R=$ constant is a region in which the distribution locally has the Sauter shape. The only case shown is for $Z=84$. For $Z=26$ the curves essentially follow the straight lines $R=1$ and even for $Z=50$ the deviations are barely significant within the errors of the calculation This was why, as was elucidated by later theoretical work, it was possible to get along with a Sauter distribution for many years—the shape was much better than the normalization. Roughly speaking, the error in the Sauter total cross section is $O(\pi a)$ (from omission of the characteristic $e^{-\pi a}$ factor) but the significant errors in the Sauter distribution are only $O(a^2)$. But Fig. 2 does show that in the heaviest elements the deviations from the Sauter distribution become significant. The rise in R at small angles occurs because the Sauter distribution, unlike an exact calculation, vanishes in the forward direction. If this were the only region which deviated from Sauter form the curve would elsewhere behave as $R=$ constant. Instead, at larger angles it falls off more slowly than the Sauter form, and indeed there is no sizeable angular region of Sauter shape. These qualitative features were first remarked in the experiments. Finally, the angle $\theta_{\max}$ of maximum emission, roughly indicated on the graphs, occurs in the region in which R is rising, so the cross section is staying up in comparison to Sauter, and so $\theta_{\max}$ is being shifted toward larger angles in comparison to the Sauter distribution. This too was first noted in the experiments.

The relative $O(a)$ corrections, mentioned earlier, do

not shed much light on these properties—they appear to be $O(a^2)$ effects. This arises, as was noted by Nagel,[27] both because at intermediate energies the $O(a)$ term is not large and because its distribution is similar to the Sauter form. There is a tendency for a maximum at larger angles and for a larger cross section at back angles, but especially for the latter effect the increase is insufficient. Nagel also pointed out that the reason the $O(a)$ distribution vanishes in the forward direction is that it arises as a cross term with the Sauter matrix element. The lowest order nonvanishing cross section in the forward direction $I(0)$ is relative $O(a^2)$, and this Nagel obtained.[43a] It has been conventional to express this in terms of the ratio $\kappa\equiv I(0)/I(\theta_{\max})$. From Table XI we would estimate that at 1332 keV, this ratio is 0.30 for Pb and 0.38 for U. These compare with the theoretical values 0.27 obtained for Pb by Sauter and Wüster[44] in a numerical calculation and 0.42 obtained by Nagel for Pb from the relative $O(a^2)$ term above. Hultberg's experimental value for κ in U at 1332 keV was 0.245, which again reflects the fact that the experimental forward cross section at the higher energies lies below theory.[45] (Some new measurements of κ have recently been reported by Rimskii-Korsakov et al.[46])

It is finally of some interest to discuss the behavior of the K-shell angular distribution in the high-energy limit. At high energies, the significant angles are $O(1/k)$, and in analytic work it is appropriate to expand in $1/k$ and θ, but for arbitrary $x\equiv k\theta$. Neglecting $O(a^2)$, Nagel[27] writes the distribution in this limit as

$$\sim \frac{x^2}{(1+x^2)^3}\left[1-a\frac{\pi}{2}\frac{1}{(1+x^2)^{1/2}}\right], \qquad (6.1)$$

including the $O(a)$ correction to the Sauter distribution which has its maximum at $x=1/\sqrt{2}$. Nagel (and also Mork and Olsen[47]) find that in this limit forward scattering is characterized by $\kappa=5.85a^2$ to lowest nonvanishing order in a. Mork and Olsen also obtained an exact expression for the forward scattering in the high-

[43a] This result was also independently obtained by Arne Reitan, Physica Norvegica 1, 113 (1961).

[44] F. Sauter and H. O. Wüster, Z. Physik 141, 83 (1955). Actually these authors obtained $I(0°)$ numerically and took $I(\theta_{\max})$ from the usual Sauter distribution, a procedure which certainly becomes invalid at high energies as will be seen shortly.

[45] Nagel (Ref. 27) compares the Sauter-Wüster 0.27 value with Hultberg's 0.245, calling the agreement rather good, apparently assuming that for large Z, κ does not change appreciably with Z. The present results do not support this assumption, and we conclude there is a significant difference between theory and experiment.

[46] K. K. Aglinstev, V. V. Mittrofanov, A. A. Rimskii-Korsakov, and V. V. Smirnov, Bull. Acad. Sci. USSR 25, 1146 (1962); A. A. Rimski-Korsakov and V. V. Smirnov, Zh. Eksperim. i Teor. Fiz. 42, 67 (1962) [English transl.: Soviet Phys.—JETP 15, 47 (1962)]; and Bull. Acad. Sci. USSR 26, 1180 (1963).

[47] K. Mork and H. Olsen, Proceedings of the Physics Seminar in Trondheim, No. 5, 1960 (unpublished).

energy limit; such an expression was also later obtained by Weber and Mullin,[48] who graph $F(0)$ against Z, where

$$F(\theta) = \frac{1}{4e^2 a^5 \epsilon} \frac{d\sigma}{d\Omega} \qquad (6.2)$$

in dimensionless units. In the high-energy limit, F is independent of energy. For Pb we would compute $\kappa = 2.1$, an absurd result ($\kappa \leq 1$) which could be interpreted as a gross failure of the expansion of $F(0)$ in a. In fact, the error lies in the supposition that the position of the maximum is given by the Sauter maximum, whereas numerical calculations of Boyer[49] and Nagel[50] show that in heavy elements the maximum occurs for forward emission and the distribution decreases monotonically. Using Nagel's calculation[50] we find that the ratio of forward emission to emission at the Sauter angle is 1.6. In Fig. 3 we plot $F(x)$ for $Z = 82$ for three of the energies of our numerical calculation and also show the high-energy limit from Nagel's work. This again makes very clear how far removed 2 MeV is from the asymptotic energy region. Even the manner in which the minimum at forward angles gets filled remains to be calculated by higher energy work. (The high-energy limit has now also been discussed by Gorshkov and Mikhailov.[51])

[48] T. A. Weber and C. J. Mullin, Phys. Rev. **126**, 615 (1962).
[49] R. H. Boyer, Ph.D. thesis, Oxford University, 1957 (unpublished).
[50] B. Nagel, Arkiv Fysik **24**, 151 (1963).

[51] V. G. Gorshkov and A. I. Mikhailov, Zh. Eksperim. i Teor. Fiz. **44**, 2142 (1963) [English transl.: Soviet Phys.—JETP (to be published)].